Acoust. Sci. & Tech. **26**, 4 (2005)

PAPER

Inversion for seabed geoacoustic properties in shallow water experiments

Kazuhiko Ohta[1,*], Kouki Okabe[1], Itaru Morishita[2], Shunji Ozaki[2] and George V. Frisk[3]

[1]*Technical Research and Development Institute, Japan Defense Agency*
[2]*Oki Electric Industry Co., Ltd.*
[3]*Woods Hole Oceanographic Institution*

(*Received 22 March 2004, Accepted for publication 10 December 2004*)

Abstract: Low frequency sound propagation features and bottom sediment properties in shallow water were studied in the Shallow Water Acoustic Technology (SWAT) experiments conducted in the East China Sea. In these experiments, a hydraulic-type acoustic source was towed over a range of some 30 km at constant mid-water depth and transmitted low-frequency cw signals, which were received on a bottom-moored vertical line array. After suppressing a time-dependent factor of the received signals, the asymptotic Hankel transform was applied to the acoustic field provided by the resulting synthetic aperture horizontal array that was created at each receiver depth. The horizontal wavenumber spectra thus obtained had peaks corresponding to mode, but these peak positions were observed to be slightly different among the different receiver depths partially due to noise and range dependency. Thus, stochastic mode inversion was exploited by using all of the identified peak positions for estimation of the geoacoustic properties. The sound field simulated using the estimated properties was compared with the measured one for each receiver depth and an excellent agreement was confirmed not only at the frequency used for the inversion but also at the different frequency.

Keywords: Geoacoustic, Shallow water, Sound propagation, Inversion method

PACS number: 43.30.Bp, 43.30.Pc [DOI: 10.1250/ast.26.326]

1. INTRODUCTION

A series of experiments were conducted on the continental shelf of the East China Sea from 1999 through 2001 as a part of SWAT (Shallow Water Acoustic Technology) project for studying the shallow water acoustic properties [1,2]. The same kind of experiment was also conducted on the New Jersey continental shelf of the Atlantic Ocean in October 2000 [3,4]. One of the major targets in this project was to estimate the subbottom geoacoustic properties such as sediment sound speed, which characterize the sound propagation in the shallow water environment. A number of inversion methods to infer the geoacoustic properties have been developed so far. Panda *et al.* [5] developed a sediment classification model to estimate the impedance and attenuation of subbottom sediments from the reflection of wideband FM pulse signals incident normally to the sea floor. Although this method is convenient owing to a small-scale measurement for survey, the accuracy of the reflection property in low grazing angle might be insufficient in shallow water, where the sound propagation is strongly affected by sediment properties due to the multiple bottom interactions. Modal inversion [6–8] is one of the most useful methods to estimate the geoacoustic properties which have an influence on the low frequency sound propagation. Once the geoacoustic parameters are specified, the reflection coefficient can be derived with respect to even very low grazing angle.

The objective of the present paper is to reasonably account for the propagation features of low frequency sound measured in the shallow water of the East China Sea in connection with subbottom acoustic properties. Since the sediment type of the experiment area is sand, which is generally difficult for high frequency sound to penetrate into the deeper subbottom, the modal inversion using low frequency sound is here employed to estimate the subbottom geoacoustic properties.

Effective employment of the modal inversion requires the accuracy of mode eigenvalues observed from the peaks of horizontal wavenumber spectrum, which can be obtained using the asymptotic Hankel transform of measured sound field. Depending on the measurement depth, however, some of the spectrum peaks on target do not have large amplitude enough to be identified, since the associated mode

*e-mail: kohta@jda-trdi.go.jp

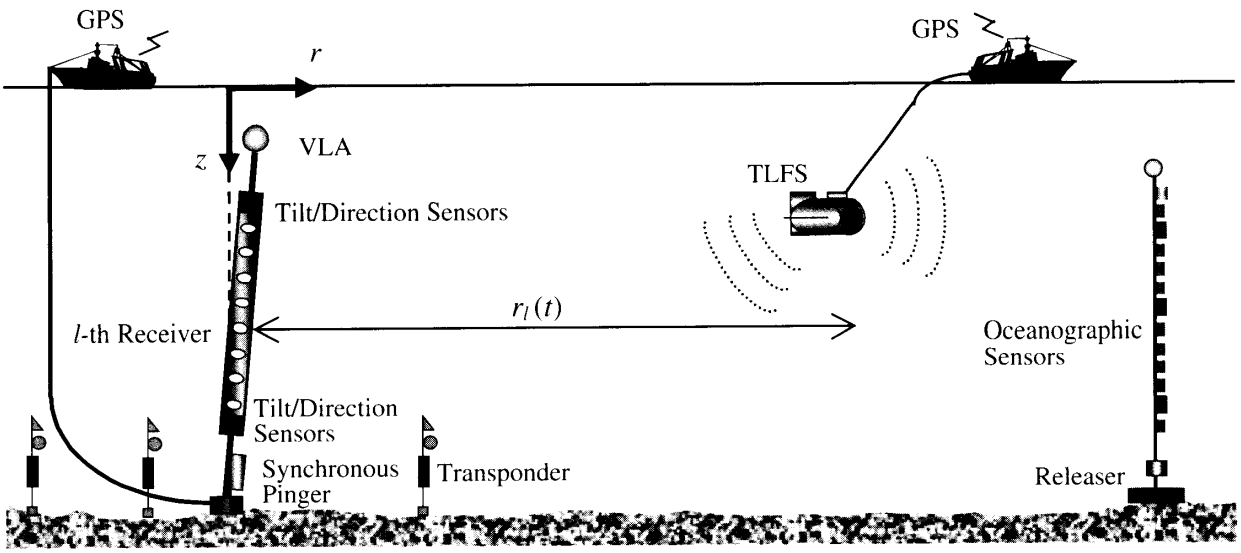

Fig. 1 Configuration of experiment conducted on the continental shelf of the East China Sea.

eigenfunctions constructing the field vary along with depth. As a result, determination of the peak position in the spectrum is hard due to noise interference, so that its accuracy might not be attained as expected. Thus, a bottom-moored vertical line array of receivers was introduced in the above geoacoustic experiment and all of the spectrum peaks observed at different receiver depths were employed in a stochastic modal inversion [6] to enhance the precision of the inversion processing.

Section 2 describes one of the experiments carried out in the shallow water of the East China Sea. Section 3 discusses the results obtained by applying the asymptotic Hankel transform to the sound fields measured by the vertical line array. In Section 4, geoacoustic bottom properties estimated using the stochastic modal inversion method are evaluated by comparison of the measured and simulated sound fields at different receiver depths. Section 5 presents concluding remarks.

2. ACOUSTIC EXPERIMENT WITH VERTICAL HYDROPHONE LINE ARRAY

The present paper focuses on an experiment conducted on the continental shelf of the East China Sea in July 1999. The purpose of this experiment is to estimate the geoacoustic sediment properties and to study the propagation features of low frequency sound. The basic configuration of the experiment is schematically illustrated in Fig. 1. The bathymetric variation of the experimental area is less than few meters as shown in Fig. 2. A vertical line array (VLA) of hydrophone receivers extended from 44 m through 86 m in depth was moored on the sea floor at a site named Q having a water depth of 104 m. The VLA consists of eight hydrophones with an equally spacing of 6 m and a set of tilt, depth and directional sensors plus thermometers

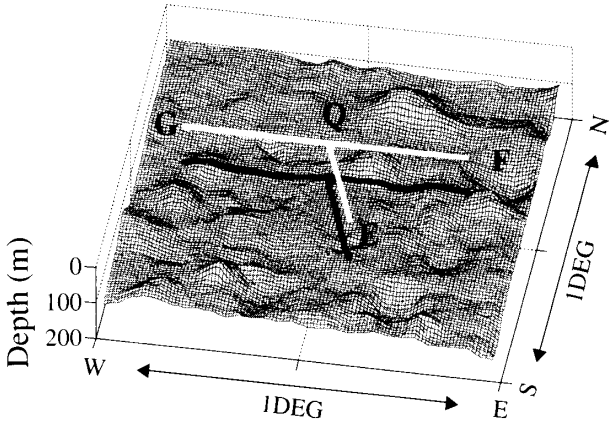

Fig. 2 Bathymetric variation of experimental area. Solid white lines indicate the tracks of the TLFS source towed by a ship.

equipped at both ends of the VLA, which is also connected to an optical fiber cable of 5 km in length. A subsurface buoy with a buoyancy of 350 kg kept the VLA vertical throughout the experiment, so that the output of the tilt sensor did not indicate more than 2–3 deg. The acoustic data collected by each hydrophone and other instruments were transmitted through the fiber cable to a ship, which was located approximately 4 km away from site Q. A pinger attached on the VLA and three transponders placed on the seafloor around it were used to precisely determine each hydrophone position in water column. This ranging system had been calibrated by measuring the position of each transponder with kinematics GPS prior to the acoustic measurement.

A sound source named TLFS [9] with transmitting continuous wave (cw) signals was towed at a depth of about 40 m by another ship, which moved at a constant

Table 1 Distribution of grain size of bottom sediment collected at site Q.

	Grain size (ϕ)	Weight ratio (%)	
Sand	−1–0	0.975	97.097
	0–1	2.746	
	1–2	14.806	
	2–3	61.993	
	3–4	16.577	
Silt	4–5	2.903	2.903
Mean grain size	2.4		

$\phi = -\log_2(L)$, L: Grain diameter (mm)

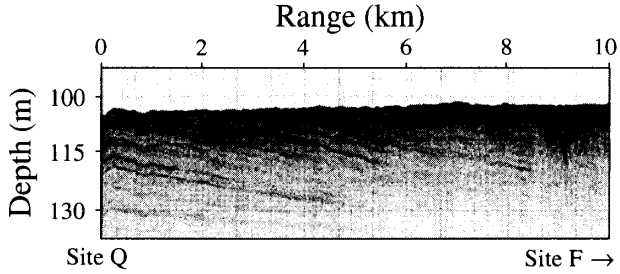

Fig. 3 Bottom sediment structure surveyed along the track Q-F by a chirp sonar.

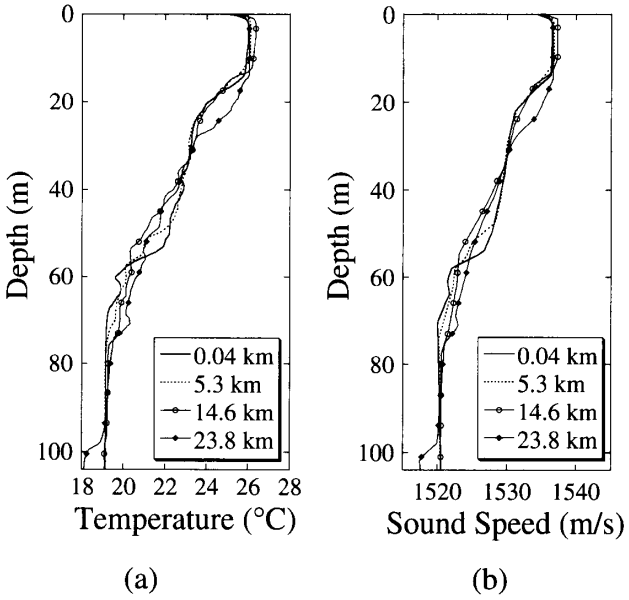

Fig. 4 Temperature profiles (a) measured by XBT in towing the TLFS source along the track Q-F and corresponding sound speed profiles (b) converted from the temperature profiles. Numerical values in legend indicate horizontal range from site Q in casting XBT. Solid line in each graph represents the profile used for modal inversion.

speed of approximately 6 knots along the tracks depicted in Fig. 2. The range of each track was about 18 nm and the water depth along the tracks was nearly constant. The TLFS source is a hydraulically driven projector whose electric power is supplied and controlled from the ship through an umbilical cable. This projector is designed to cover a frequency range of 20 through 200 Hz, and to exceed 181 dB re 1 μPa@1 m (hereafter described "dB") at 20 Hz and 187 dB in the frequency range from 50 through 200 Hz. Commands were sent from the controller on board to the projector, which can be remotely monitored in real time. Since several kinds of sensors were installed in the projector, the posture and depth of the projector together with environment condition can be measured and recorded on board. The TLFS source remained stable when being towed and its depth variation was less than 1 m.

Prior to the acoustic measurements, the surficial bottom sediment properties in the experimental area were examined by collecting gravity cores, which was nevertheless limited to tens of centimeters below the sea floor. This is due to the fact that the sediment of the experimental area is primarily composed of sand, which is found from distribution of grain size of the surficial sediment at site Q as indicated in Table 1. The bathymetry and sediment structure were also investigated using a chirp sonar, which consisted of eight hydrophones and single transducer with a source level of 197 dB and a frequency range of 2–7 kHz. The chirp sonar was towed at a speed less than 4 knots but could be submerged no further than 10–15 m below the sea surface. Due to the inadequacy of its acoustic power and the sandy sediment, the chirp signal could not penetrate more than 20 m into the sediment. Processed chirp data along the track Q-F identify several subbottom layers as represented by Fig. 3. These individual layers are considered to be the result of repeated growth and regression of the paleoshoreline during glacial and inter-glacial periods.

In the acoustic measurement, the ship also conducted oceanographic measurements using XBTs (Expendable Bathy Thermometer) frequently and the temperature profiles measured during the movement from site F to site Q are displayed in Fig. 4(a). The sound speed profiles (SSP) converted from these temperature profiles are also presented in Fig. 4(b) [10]. In addition, a couple of vertical chains equipped with self-recording sensors for temperature, salinity, conductivity, and current velocity/direction were moored on the sea floor. These oceanographic monitoring chains were deployed near site Q and the other limit of the tracks throughout the experiment. Figure 5 shows the time variation of the outputs of sensor near the VLA over three days. The water temperature was observed to vary stronger with getting closer to the sea surface. The temporal variation of the current velocity and direction was found to be affected by the tidal variation.

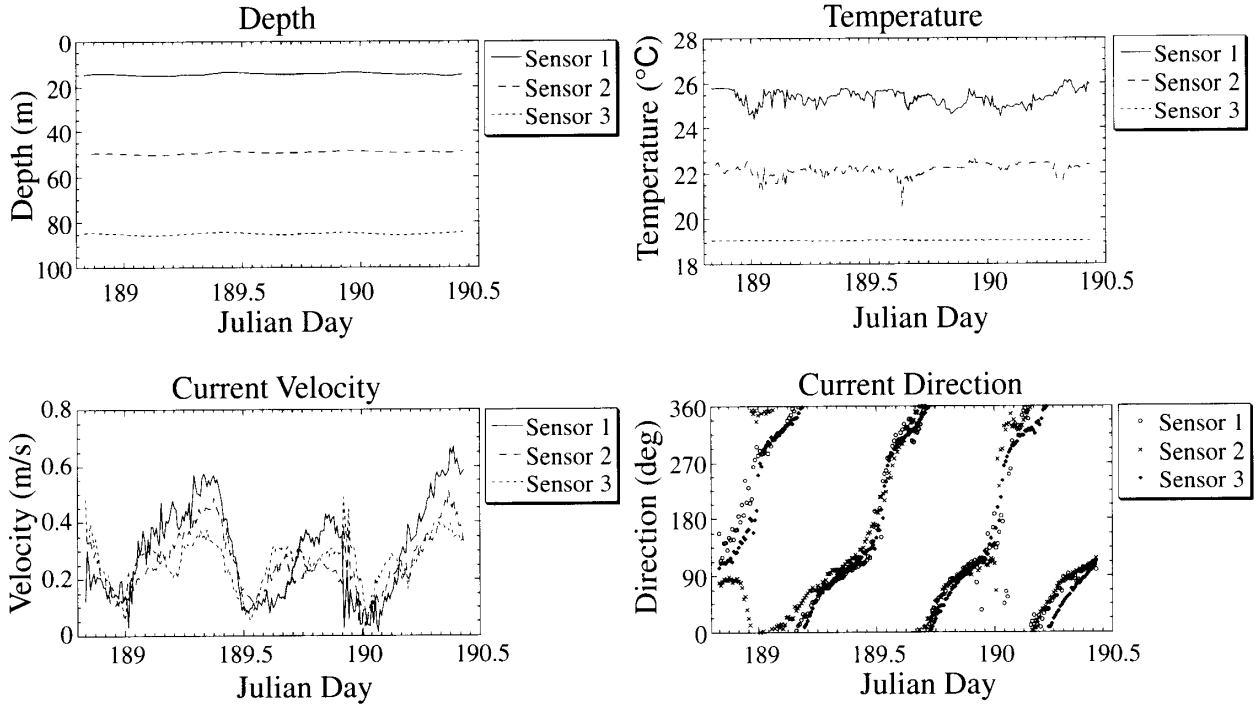

Fig. 5 Temporal variation of sensor depth, temperature, current velocity and direction which were measured by oceanographic monitoring chain deployed near site Q. The shaded area indicates a time period of acoustic measurement in towing the TLFS source along the track Q-F.

3. DETECTION OF MODE EIGENVALUES

For a coordinate system such that z is depth measured vertically downward from the sea surface and r is horizontal range from the VLA position as shown in Fig. 1, the acoustic pressure measured by the l-th VLA-hydrophone at a depth of z_l $(1 \leq l \leq 8)$ at t_j in time is described as $\bar{p}_l(t_j, r(t_j))$ for the source located at a position of $(r(t_j), z_s)$, where both z_s and z_l are assumed to be constant. From the measured pressure $\bar{p}_l$, we can derive the acoustic field $p(r, z_l; z_s)$ on the resulting synthetic aperture horizontal array due to the moving source as $p = \bar{p}_l(t_j, r(t_j))e^{-i2\pi f(t_j - t_0)}$, where f is a constant frequency of the source and t_0 is some fixed time. The zeroth-order asymptotic Hankel transform of the acoustic field p yields a depth-dependent horizontal wavenumber spectrum g_l as

$$g_l(k_r) \approx \frac{e^{i\pi/4}}{\sqrt{2\pi k_r}} \int_{-\infty}^{\infty} p(r, z_l; z_s) e^{-ik_r r} \sqrt{r} dr, \qquad (1)$$

in which k_r is the horizontal wavenumber and i is an imaginary number [11]. The mode eigenvalues can then be determined from the peak position of $\sqrt{k_r}|g_l(k_r)|$ for the horizontally stratified media including bottom sediments.

To obtain mode eigenvalues in a weakly range-dependent environment, a short sliding window $w_\Lambda(r; \hat{r})$ with length Λ and center position $\hat{r}$ may be introduced in Eq. (1) in analogy with a short time Fourier transform (STFT) as follows:

$$g_l(k_r) \approx \frac{e^{i\pi/4}}{\sqrt{2\pi k_r}} \int_{-\infty}^{\infty} w_\Lambda(r; \hat{r}) p(r, z_s; z_l) e^{-ik_r r} \sqrt{r} dr, \qquad (2)$$

where $p(r, z_s; z_l)$ is assumed to be equivalent to $p(r, z_l; z_s)$ on the basis of the reciprocity principle between the source and receiver positions [8]. Here, the Kaiser-Bessel window [12] is actually used so as to effectively minimize the interference of adjacent peaks of spectrum effectively. Considering a Doppler effect due to the movement of the source, the eigenvalue of Mode m can be related to the following $k_m^{(l)}$ (hereafter called "modal peak"):

$$k_m^{(l)} = \frac{2\pi f \hat{k}_m^{(l)}}{2\pi f - \hat{k}_m^{(l)} v}, \qquad (3)$$

where v is the speed of the moving source and $\hat{k}_m^{(l)}$ is the above peak position in $\sqrt{k_r}|g_l(k_r)|$.

As a representative example of accomplishments, Fig. 6 shows the range-dependent evolution of spectra obtained by applying the Hankel transform in Eq. (2) with $\Lambda = 5$ km to the synthetic aperture due to the source moving along the track Q-F, where the source frequency in use was 25 Hz. The center position of the window was slid every 0.5 km. The less range dependency of the acoustic media near site Q is seen from this figure. The horizontal wavenumber spectra at different receiver depths over the range of 0.5–5.5 km on the same track are also shown in Fig. 7. The water depth over this range period has a small variation and its mean value is about 103 m. The modal

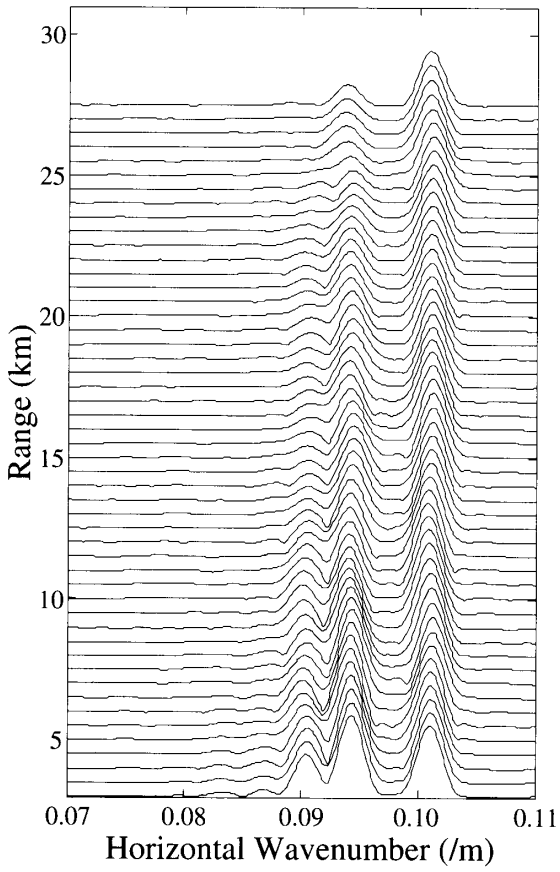

Fig. 6 Range-dependent evolution of the output wavenumber spectrum obtained by applying the zeroth-order asymptotic Hankel transform with a sliding Kaiser-Bessel window of 5 km length to the synthetic aperture due to source towed along the track Q-F by transmitting cw sound of 25 Hz. The range represents the center position of the sliding window. The depths of source and receiver used for this analysis are 40 m and 44 m, respectively.

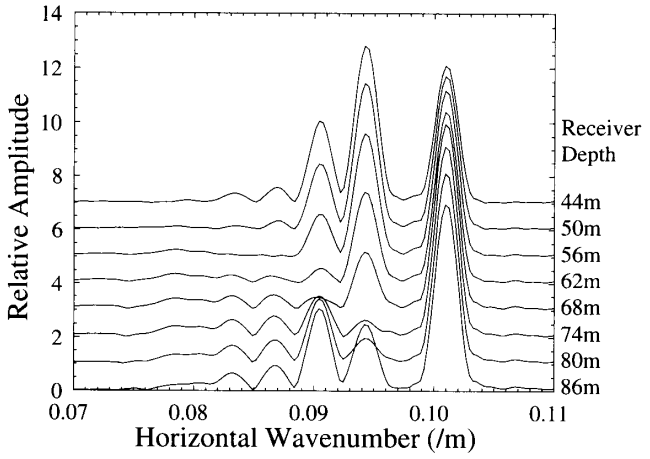

Fig. 7 Comparison of depth-dependent wavenumber spectra at different receivers of VLA. Each spectrum was obtained by applying the zeroth-order asymptotic Hankel transform to the synthetic aperture over 0.5–5.5 km in range along the track Q-F.

peaks identified in Fig. 7 correspond to Modes 1 through 5. Theoretically, the peak positions corresponding to the same mode must be identical over the different receivers, but the observed ones actually have slight discrepancies each other as indicated in Table 2. These discrepancies can be accounted for partially by noise influence when the field is measured at the depth close to the node of the mode on target and partially by range dependency of media including the water column. As seen from Fig. 7, a part of the peaks are too hard to identify, thus being denoted by bars in Table 2.

4. STOCHASTIC MODAL INVERSION RESULT

A set of modal peaks detected in the previous section can serve to estimate the sound speed in the sediment by employing the modal inversion method [7], which is based on the perturbative relation between mode eigenvalues and sound speed. Since the observed positions of the modal peaks corresponding to the same mode, however, are not completely equivalent as indicated in Table 2, an error in the observation may be introduced in the perturbative relation as

$$\boldsymbol{d} = \boldsymbol{G}\boldsymbol{q} + \boldsymbol{u}, \tag{4}$$

with

$$\boldsymbol{q}(n) = c(z_n) - c_0(z_n),$$

$$\boldsymbol{d}(m + M(l-1) - \mu) = k_m^{(l)} - k_m^{(0)},$$

$$\boldsymbol{u}(m + M(l-1) - \mu) = u_m^{(l)},$$

$$\boldsymbol{G}(m + M(l-1) - \mu, n) = -\frac{4\pi^2}{k_m^{(0)}\rho(z_n)} |\phi_m^{(0)}(z_n)|^2 \frac{f^2}{c_0^3(z_n)} \Delta z,$$

where z_n: discrete depth in sediment subject to inversion ($1 \le n \le N$), Δz: depth increment, $c(z)$: sediment sound speed to be estimated, $c_0(z)$: initial sediment sound speed provided arbitrarily, $k_m^{(0)}$: m-th mode eigenvalue derived numerically using the initial sound speed, $\phi_m^{(0)}$: m-th mode eigenfunction derived numerically using the initial sound speed, $u_m^{(l)}$: error in observation of $k_m^{(l)}$, ρ: sediment density, M: maximum mode number in the identifiable modal peaks, and μ: number counted up when the modal peak is unidentified as denoted by the bars in Table 2.

To solve Eq. (4) for the vector $\boldsymbol{d}$, the following stochastic inversion method [6] was applied:

$$\boldsymbol{q} = \boldsymbol{Y}\boldsymbol{G}^{\mathrm{T}}(\boldsymbol{G}\boldsymbol{Y}\boldsymbol{G}^{\mathrm{T}} + \boldsymbol{S})^{-1}\boldsymbol{d}, \tag{5}$$

where $\boldsymbol{Y}$ and $\boldsymbol{S}$ represent covariance matrices of $\boldsymbol{q}$ and $\boldsymbol{u}$, respectively, and T superscript denotes transpose. By assuming that the errors in each observation of the modal peaks are uncorrelated, $\boldsymbol{S}$ is provided by a diagonal matrix composed of the square of $\sigma_m^{(l)}$, which is the standard deviation of $u_m^{(l)}$ and is obtained by $\sigma_m^{(l)} = \pi/\Lambda\sqrt{SNR_m^{(l)}}$ with

Table 2 Measured modal peak positions in the depth-dependent horizontal wavenumber spectra and eigenvalues calculated by using the estimated sound speed of the sediment. Bar denotes the case where the modal peak was too small to be identified. The values in parenthesis were not utilized for the stochastic modal inversion due to large deviation from averaged one.

Receiver depth (m)	Mode 1	Mode 2	Mode 3	Mode 4	Mode 5
44	0.101007	0.0942870	0.0905080	0.0869113	0.0833775
50	0.101007	0.0942865	0.0905157	0.0869886	(0.0835176)
56	0.101008	0.0942863	0.0905323	—	—
62	0.101008	0.0942840	0.0905928	(0.0864158)	0.0830796
68	0.101009	0.0942796	(0.0902267)	0.0866287	0.0831513
74	0.101009	0.0942549	0.0904310	0.0867001	0.0831864
80	0.101009	0.0943172	0.0904582	0.0867448	0.0832005
86	0.101010	0.0942968	0.0904695	0.0867778	0.0832042
Calculated eigenvalue	0.101003	0.0942765	0.0904653	0.0868028	0.0831682

$SNR_m^{(l)}$, observed S/N ratio of each modal peak [7]. On the other hand, $\boldsymbol{Y}$ is here given by $\boldsymbol{Y}(n,n') = \sigma_n^2 \exp[-((n-n')\Delta z/\eta)^2]$ between z_n and $z_{n'}$ $(1 \le n' \le N)$, σ_n and η are the standard deviation and correlation length of $\boldsymbol{q}$, respectively.

To derive both $k_m^{(0)}$ and $\phi_m^{(0)}$, the SSP in the water column at $r = 0.04$ km is selected and is assumed to be range-independent in view of the fact that the property in the water column is relatively stable as seen from comparison with the SSP at 5.3 km (see Fig. 4(b)). Actually, the temporal variation in the water column was considerably gentle during the time period when TLFS was towed from site F to site Q as indicated by hatch in Fig. 5.

With support of Hamilton's result [13] in addition to the coring and chirp sonar analyses, we assumed $\rho = 1.7$ g/cm^3 and the initial sediment SSP represented by the straight dashed line in Fig. 8(a). Here, the density was treated to be constant throughout the sediment subject to the inversion, since its variation does not affect the sound propagation features as strongly as the sound speed variation in sediment [14].

From these SSPs in the water and sediment columns, both $k_m^{(0)}$ and $\phi_m^{(0)}$ were derived numerically by KRAKEN [15], that is, a propagation model based of the mode theory. For $k_m^{(l)}$ required in Eq. (5), the observed no-unique modal peaks were all employed except for those with large deviation such as indicated in parenthesis in Table 2.

As a result of executing Eq. (5) with $\Delta z = 3$ m, $c(z_n)$ were obtained as represented by dots in Fig. 8(a). Here, it was assumed that $\sigma_n = 10$ and $\eta = 0$, resulting in a simple diagonal matrix composed of σ_n for $\boldsymbol{Y}$. Namely, we did not impose a smoothness constraint on the solution for the inversion. To increase the inversion accuracy, a linear fit to those dots was employed as a new initial SSP and the above inversion process was repeated. As a result of iterations, we derived a linear fitted profile such as indicated by SSP1 (solid line) in Fig. 8(a). As an

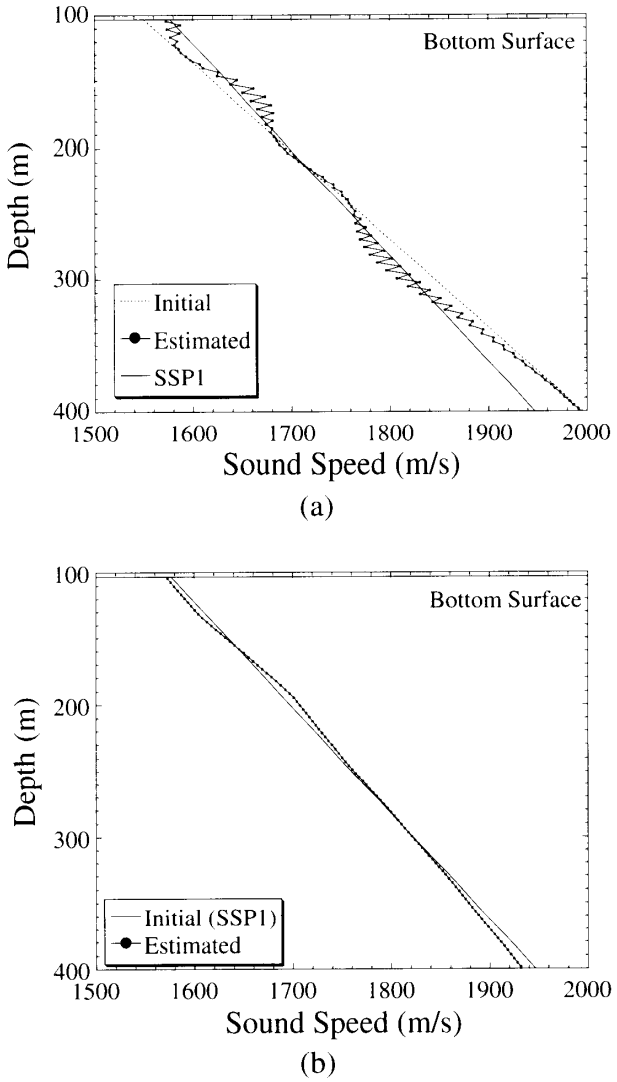

Fig. 8 Estimated and initial sound speeds in modal inversion: First (a) and iterated (b) inversion results. The solid line named SSP1 in (a) indicates a linear fit to the speeds estimated using the inversion repeatedly and is utilized as an initial sound speed for the subsequent inversion in (b).

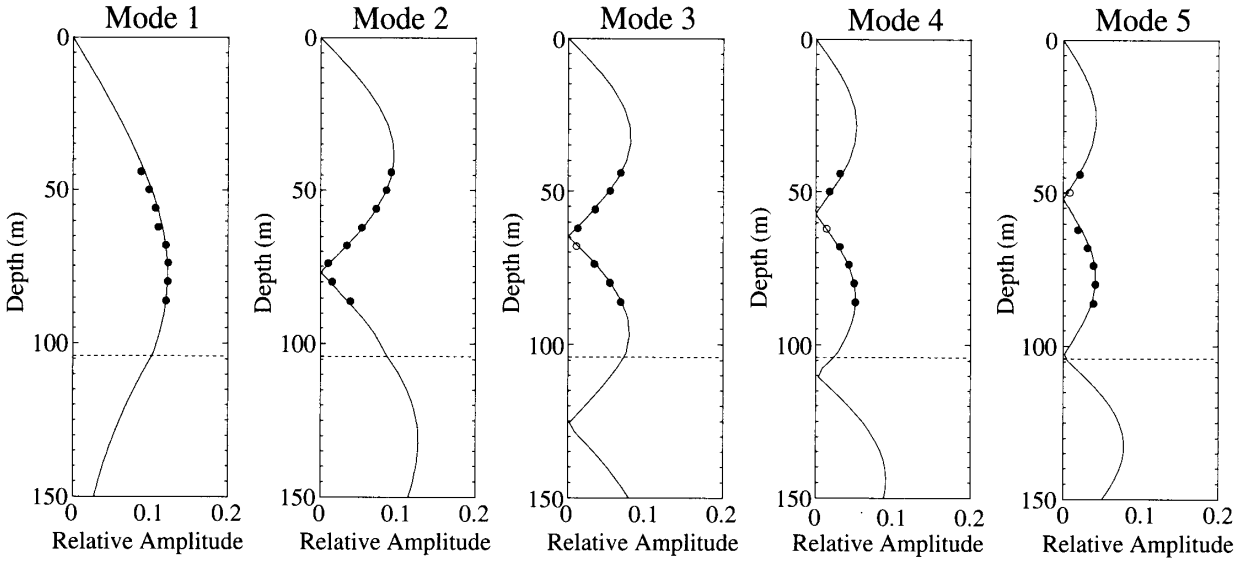

Fig. 9 Comparison of calculated eigenfunction of 25 Hz sound (solid line) and amplitude of spectrum peak (closed circle) measured at each receiver depth of VLA. Both are scaled to facilitate comparison. Broken line indicates the depth of bottom surface.

alternative approach without resorting to the linear fitting process in each iteration, a profile similar to SSP1 was also able to be attained directly from Eq. (5) by setting $\eta = 10{,}000$, which means to extensively intensify the smoothness. The use of SSP1 as an initial sound speed profile led to $c(z_n)$ indicated by dots in Fig. 8(b), which reveals that the estimated sound speed stays close to the initial profile as compared to the first inversion in Fig. 8(a).

As indicated in the lowest row of Table 2 and Fig. 9, both eigenvalues and eigenfunctions are calculated by using the estimated sediment SSP, which is represented by a sequence of linear fits to the dots in Fig. 8(b). In Fig. 9, the spectrum amplitude of modal peak at each receiver depth is scaled and compared with the corresponding eigenfunction, whose variation can well account for the depth dependency of the observed spectrum peaks.

The acoustic fields simulated using the estimated SSP in KRAKEN are then compared with the measured ones in Fig. 10(a) (initial 6 km) and Fig. 10(b) (full range), where these two fields are represented in the form of propagation loss: $-20\log_{10}|p(r, z_s; z_l)|$, due to a point source of unit amplitude at $r = 1$ m. For the simulation, the sediment attenuation α was provided on the basis of references [16–18] as $\alpha = \kappa \bar{f}^{\xi}$ (dB/m) with $\bar{f} = f/1{,}000$; these two parameters κ and ξ were here set by referring to the lateral trend of the sound propagation losses measured at plural frequencies, resulting in $\kappa = 0.1$ and $\xi = 1.25$. The simulated and measured fields agree well at each receiver depth, but show a small discrepancy beyond 6 km in range, which is outside the window used in the Hankel transform. This must be due to range-dependency of the sediment geoacoustic properties, since the lateral variation of the water temperature is not so strong as to account for the discrepancy (see Fig. 4). Although the subbottom layer structure shown in Fig. 3 does not look horizontally stratified even in the range less than 6 km, the low frequency sound employed here is less sensitive to the degree of the inhomogeneity observed in the upper portion of the sediment by the chirp sonar.

It is also observed that each field in Fig. 10 has a different interference pattern. This is due to the fact that the combination of modes which dominate the total field varies depending on the receiver depth. For example, the receiver at a depth of 62 m is close to the node of Mode 3 as seen from Fig. 9, so that a bimodal interference pattern caused by Modes 1 and 2 can be recognized in Fig. 10. Actually, the skip distance defined by $2\pi/\Delta\kappa$, where $\Delta\kappa$ is the difference between the eigenvalues of Modes 1 and 2, is 1,079 m, which accounts for the interference pattern of the field at the receiver depth of 62 m. On the contrary, the receiver at 74 m is close to the node of Mode 2 and thus the sound field at this depth indicates the shorter skip distance of 596 m due to the interference of Modes 1 and 3.

The estimated geoacoustic properties were also examined by comparison of the measured and simulated sound fields at another frequency of 40 Hz along the same track Q-F. As shown in Fig. 11, these fields are again in excellent agreement at each receiver depth. Here, bilateral modal interference can be observed at all receiver depths except 68 and 74 m, both of which are too close to the node of Mode 2 to form it as seen from Fig. 12. This result also demonstrates a fair degree of coincidence between the scaled spectrum amplitude of modal peaks and the corresponding eigenfunctions.

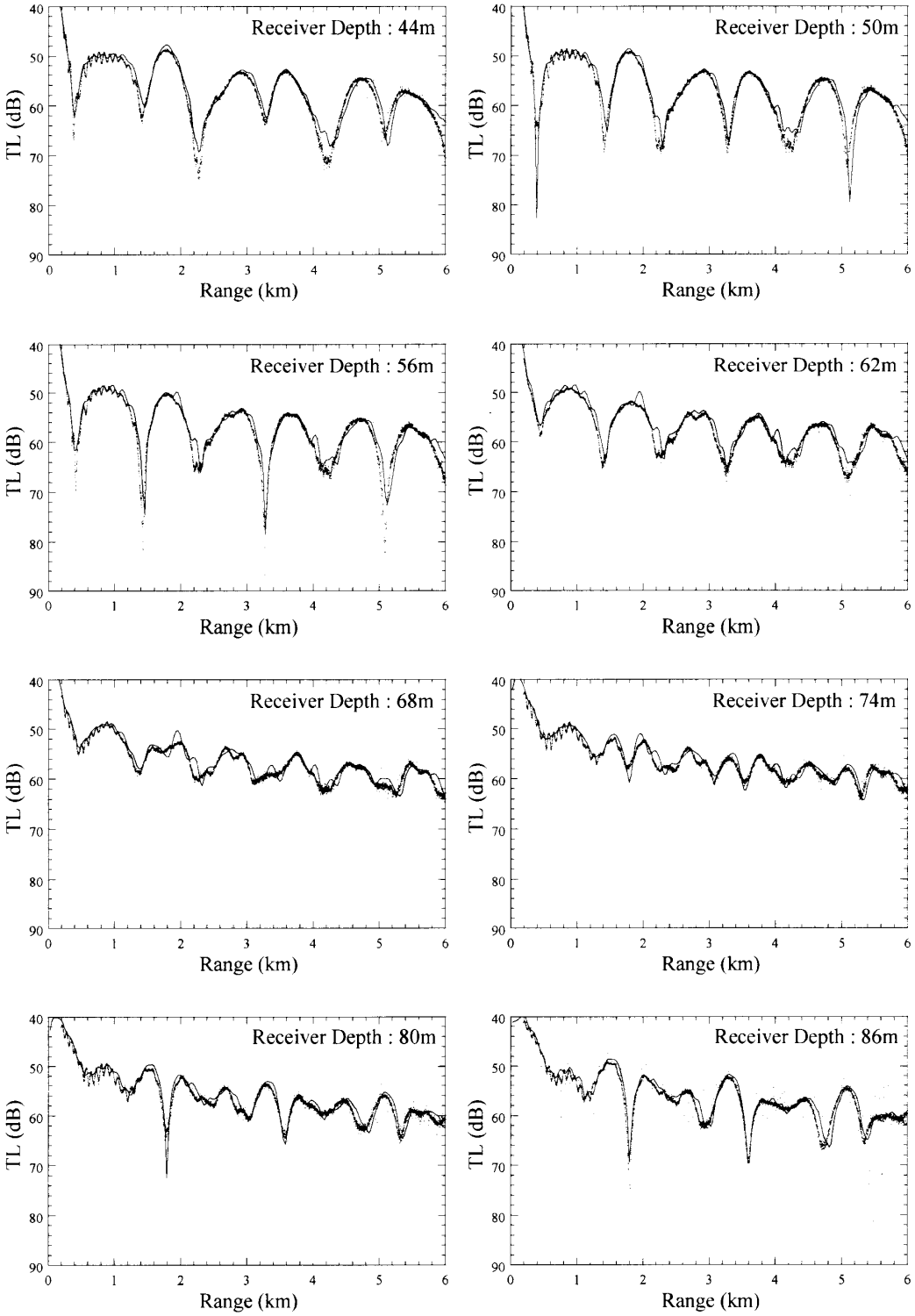

(a)

Fig. 10(a) Comparison of measured (dot) and simulated (solid line) fields of 25 Hz sound at each receiver depth of VLA along the track Q-F. Source depth was 40 m. The simulation was made by using the estimated sound speed in bottom sediment. (a) Initial 6 km and (b) full range.

It is recognized in the far range that the disagreement of the interference pattern between the measured and simulated fields at 25 Hz is larger than that at 40 Hz. Since the subbottom thickness affecting the sound field in water column increases inversely with the frequency, this observation suggests that the deeper portion of the sediment has relatively stronger range dependency. Entirely, the influence of bottom interaction in this experimental area can be properly grasped to give explanation of the propagation characteristics of low frequency sound.

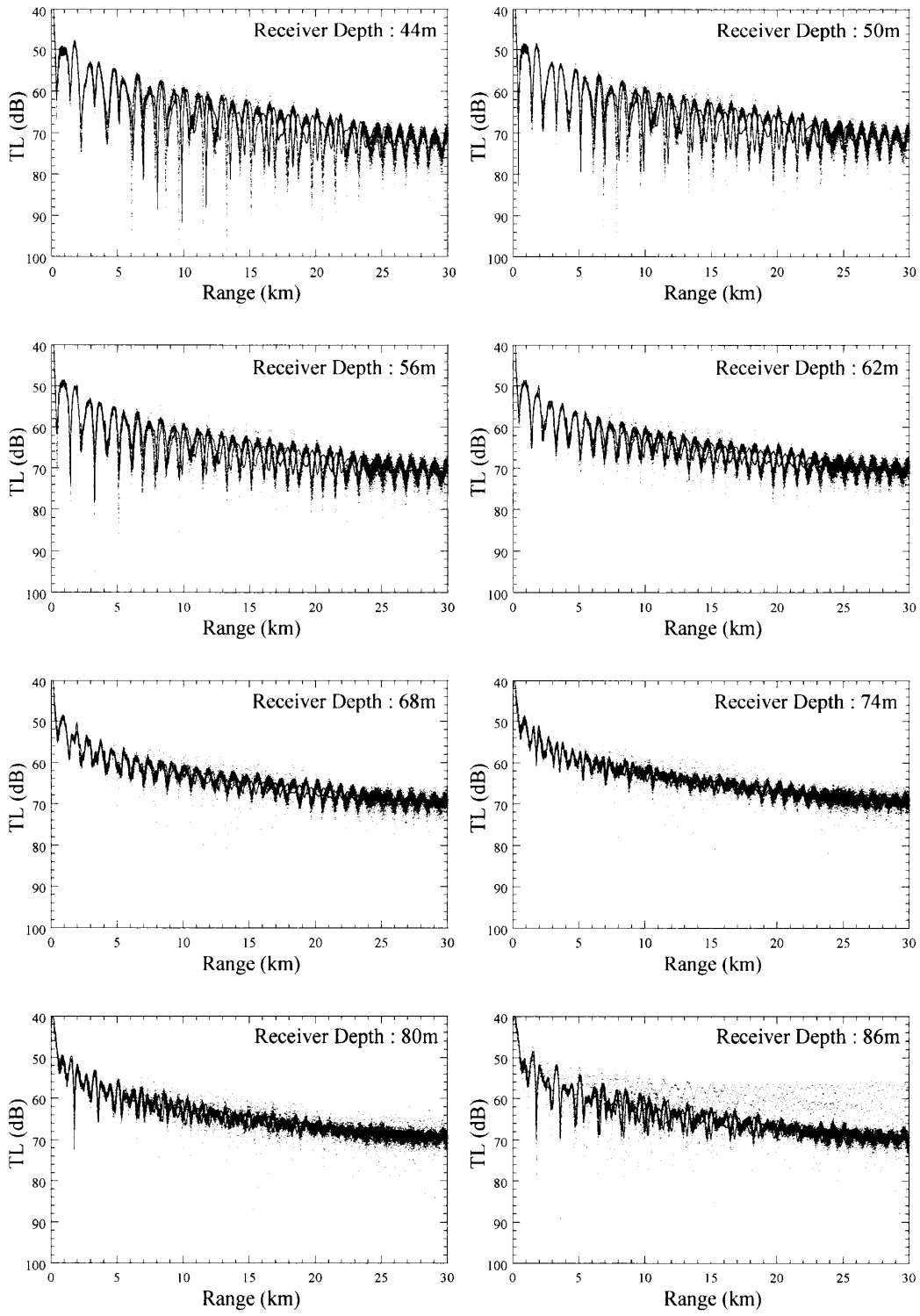

(b)

Fig. 10(b) continued.

5. CONCLUSIONS

In an attempt to estimate inversely the subbottom sediment properties in shallow water, the acoustic experiment was conducted on the relatively flat shelf with a water depth of about 100 m in the East China Sea. In this experiment, the vertical line array of receivers was moored on the sea floor and the hydraulically driven source was towed at constant depth by transmitting the low frequency cw signal of more than 180 dB in source level. To obtain the depth-dependent horizontal wavenumber spectra from each receiver output, the zeroth-order asymptotic Hankel transform with a Kaiser-Bessel short sliding window was applied to the acoustic fields measured on the resulting

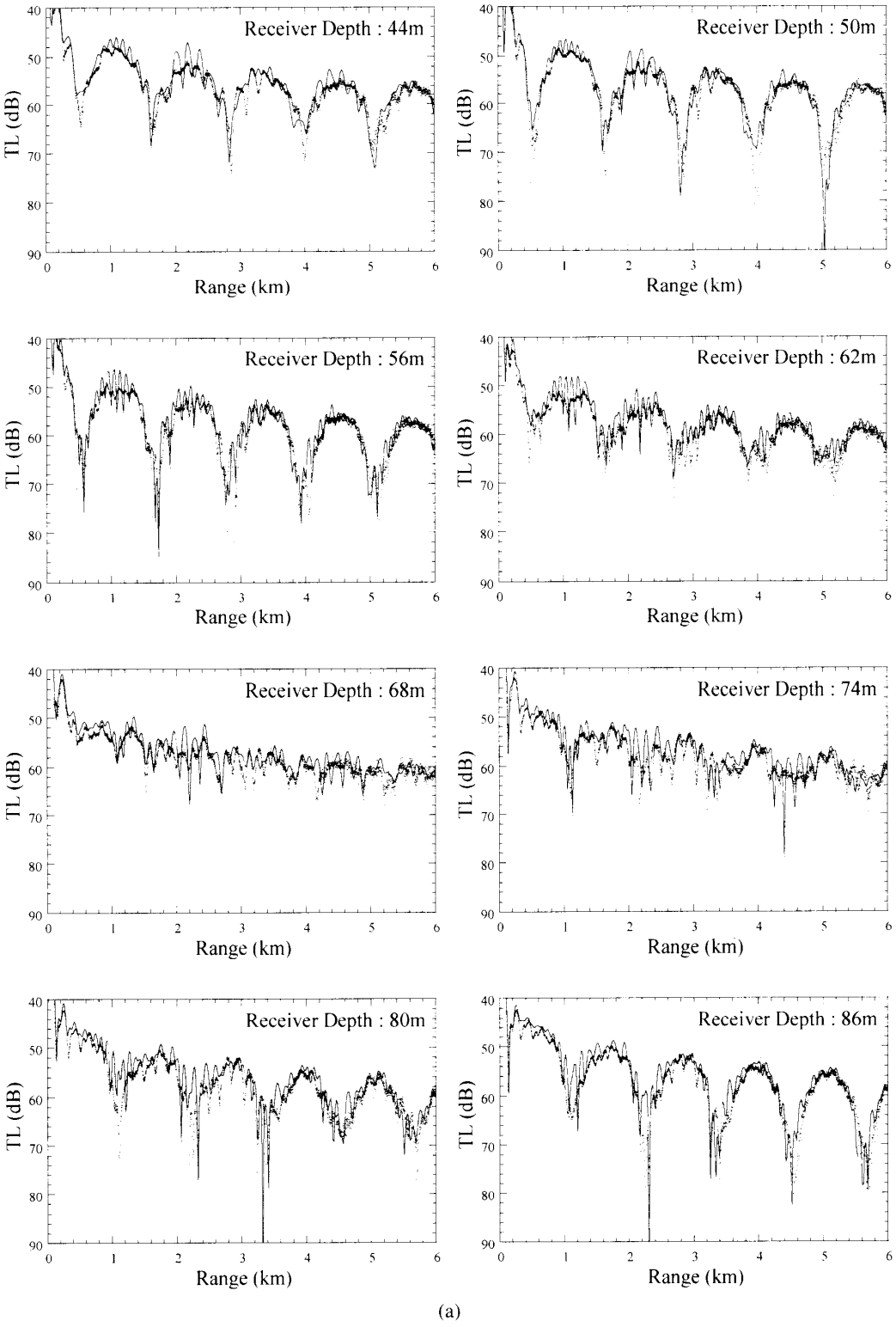

Fig. 11 Comparison of measured (dot) and simulated (solid line) fields of 40 Hz sound at each receiver depth of VLA along the track Q-F. Source depth was 40 m. The simulation was made by using the estimated sound speed in bottom sediment. (a) Initial 6 km and (b) full range.

synthetic aperture horizontal array due to the moving source. As a result of analysis of the 25 Hz sound field in a range of 0.5 through 5.5 km from the vertical array site, five spectral peaks corresponding to Modes 1 through 5 were observed. Although these modal peak positions observed at the different receiver depths must be theoretically identical and equivalent to eigenvalue of the corresponding mode, a small amount of discrepancies were recognized among them. This is considered partially due to the range dependency of environment and noise; the latter is

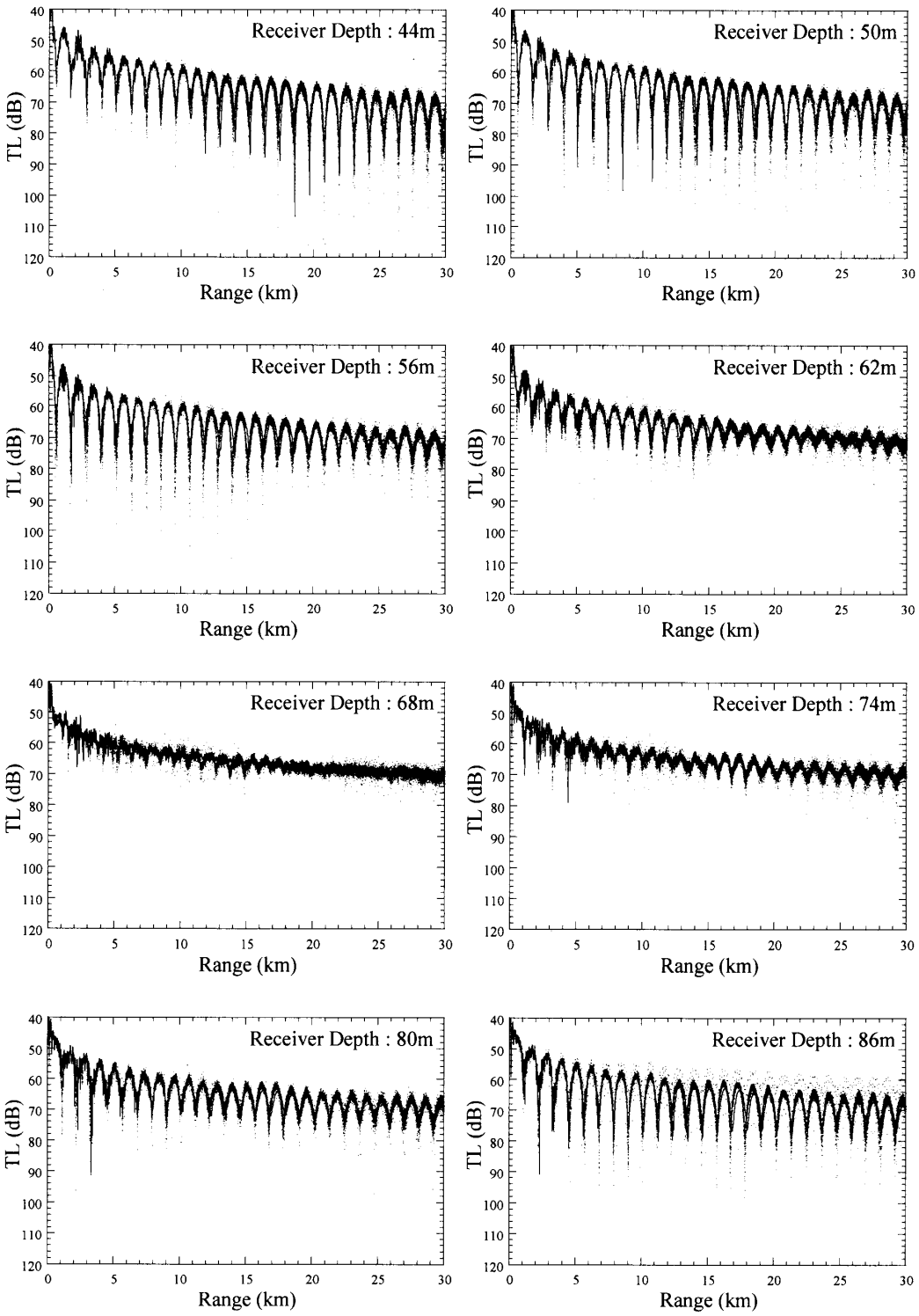

(b)

Fig. 11(b) continued.

significant when the receiver depth is close to the node of the mode.

All of the identifiable modal peaks in each spectrum were thus employed in the stochastic modal inversion to improve the estimation of the geoacoustic parameters. It is demonstrated that the sound field simulated using the inversion results agrees well with the measured one at each receiver depth. Besides, the estimated geoacoustic properties can well account for the propagation features measured at another frequency, 40 Hz.

For further studies, the range variation of geoacoustic properties will be examined using the mode range evolution observed by sliding the short window in the Hankel transform. In addition, the bottom properties along

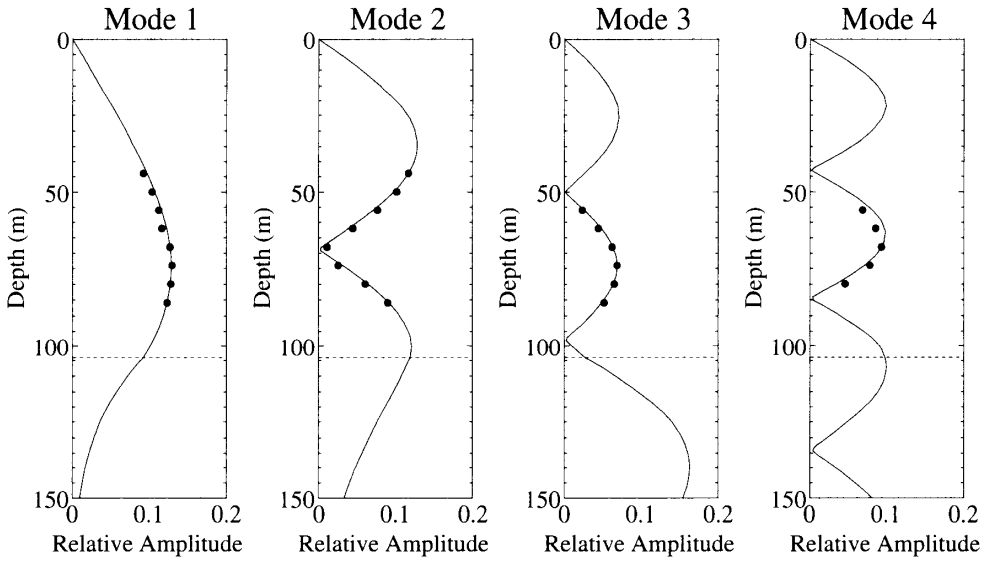

Fig. 12 Comparison of calculated eigenfunction of 40 Hz sound (solid line) and amplitude of spectrum peak (closed circle) measured at each receiver depth of VLA. Both are scaled to facilitate comparison. Broken line indicates the depth of bottom surface.

the different tracks will be also compared each other so as to understand their directional variation.

ACKNOWLEDGEMENTS

The authors gratefully acknowledge valuable discussion with Edward Franchi, Robert L. Field, and Altan Turgut, NRL for their help in the evaluation of the experimental data and analytical results.

REFERENCES

[1] S. Matsumoto, K. Ohta, K. Okabe and G. Takei, "Geoacoustic inversion using SA in East China Sea experiment," *Proc. Underwater Technology 2002 IEEE (UT2002)*, pp. 265–270 (2002).

[2] A. Turgut, D. Lavoie, D. Lambert, D. Walter and K. Ohta, "Chirp sonar inversion results from SWAT East China Sea and New Jersey Shelf," *J. Acoust. Soc. Am. Suppl.*, **109**, S2395 (2001).

[3] S. Matsumoto and K. Ohta, "Study on range-dependent evolution of the mode eigenvalue by using the Wigner distribution function," *Jpn. J. Appl. Phys.*, **43**, 3127–3130 (2004).

[4] K. Ohta, K. Okabe, M. Oikawa, I. Morishita, H. Murakami and G. V. Frisk, "Modal inversion results for geoacoustic properties in the SWAT experiments," *J. Acoust. Soc. Am. Suppl.*, **112**, S2283 (2002).

[5] S. Panda, L. R. LeBlanc and S. G. Schock, "Sediment classification based on impedance and attenuation estimation," *J. Acoust. Soc. Am.*, **96**, 3022–3035 (1994).

[6] K. Aki and P. G. Richards, *Quantitative Seismology: Theory and Methods* (Freeman, San Francisco, 1980).

[7] S. D. Rajan, J. F. Lynch and G. V. Frisk, "Perturbative inversion methods for obtaining bottom geoacoustic parameters in shallow water," *J. Acoust. Soc. Am.*, **82**, 998–1017 (1987).

[8] K. Ohta and G. Frisk, "Modal evolution and inversion for seabed geoacoustic properties in weakly range-dependent, shallow-water waveguides," *IEEE J. Ocean. Eng.*, **22**, 501–521 (1997).

[9] M. Sonehara, M. Mutoh, A. Hayakawa, F. Satoh, K. Ohta, K. Okabe, K. Ohkawa and M. Oikawa, "Exploratory development of low frequency hydraulic-type sound source," *J. Mar. Acoust. Soc. Jpn.*, **30**, 35–40 (2003).

[10] K. V. Mackenzie, "Nine term equation for sound speed in the oceans," *J. Acoust. Soc. Am.*, **70**, 807–812 (1981).

[11] G. V. Frisk, *Ocean and Seabed Acoustics: A Theory of Wave Propagation* (PTR Prentice-Hall, Englewood Cliffs, N.J., 1994).

[12] F. J. Harris, "On the use of windows for harmonic analysis with the discrete Fourier transform," *Proc. IEEE*, **66**, 51–83 (1978).

[13] E. L. Hamilton and R. T. Bachman, "Sound velocity and related properties of marine sediments," *J. Acoust. Soc. Am.*, **72**, 1891–1904 (1982).

[14] M. D. Collins, W. A. Kuperman and H. Schmidt, "Nonlinear inversion for ocean-bottom properties," *J. Acoust. Soc. Am.*, **92**, 2770–2783 (1992).

[15] M. Porter, *The KRAKEN Normal Mode Program*, Rep. SM-245 (SACLANT Undersea Research Center, La Spezia, Italy, 1991).

[16] E. L. Hamilton, "Compressional-wave attenuation in marine sediments," *J. Geophys.*, **37**, 620–646 (1972).

[17] E. L. Hamilton, "Acoustic properties of the sea floor: A review," in "Ocean Acoustic Modeling," *Proc. Conf. held at SACLANTCEN*, Pt. 4, 18-1 (1975).

[18] H. Otsubo, K. Ohta and S. Ozaki, "Normal-mode solution in the ocean with absorbing bottom sediments which have a sound-speed gradient," *J. Acoust. Soc. Jpn. (E)*, **1**, 47–57 (1980).